Progress In Electromagnetics Research C, Vol. 91, 1–13, 2019

Electromagnetic Wave Scattering from an Infinite Periodic Array of Hollow Conducting Circular Cylinders of Finite Length

Hongchang An[1] and Akira Matsushima[2, *]

Abstract—An effective numerical technique is demonstrated for the plane wave scattering from an infinite periodic array of hollow circular cylinders of finite length. The cylinders are made of infinitely thin perfect conductor and allocated in the axial direction. We formulate the boundary value problem into a set of integral equations for the unknown electric current densities flowing in the circumferential and longitudinal directions. Employment of the Galerkin method allows us to solve simultaneous linear equations for the expansion coefficients of the unknown current, from which we can find the field distributions in both far and near regions. The procedure of analytical regularization makes the linear system into the Fredholm second kind that is contributory to stable and rapidly convergent results. Resonance is detected as abrupt changes in the total scattering cross sections for each grating mode, and it is accompanied by the formation of circular cavity mode pattern in the cylinder.

1. INTRODUCTION

A hollow cylinder of finite length having circular cross section is one of the fundamental shapes in wave scattering problems and has been treated by a lot of analytical and numerical methods. The Wiener-Hopf technique, which had been originally applicable to only semi-infinite geometries, was extended to a finite circular cylinder with acoustically hard boundary [1] or electromagnetically conducting one [2, 3]. On the other hand, spread of high-speed digital computers activated the development of various numerical approaches, the important one of which is to reduce the boundary value problems into integral equations for unknown surface current density functions [4–7]. Here, the discretization scheme is based on the methods of moments [8], and efficiency and reliability of the solution depend on the skills of processing kernel and unknown functions. In this respect, the treatment by Lucido et al. [7] is particularly excellent, where the system of linear equations has the form of the Fredholm second kind as the result of analytical regularization procedure [9].

Besides an isolated body, an infinite number of cylinders periodically allocated in the axial direction also constitute an interesting and attractive system of scatterers, considering that such structures are simple models of antennas with slot arrays [10] or corrugated surfaces [11, 12], as well as metamaterial absorbers [13–15]. As a semi analytical solution, the method of Riemann-Hilbert boundary value problem was applied to an axially periodic array of hollow conducting cylinders as an eigenvalue problem without excitation [16]. The present paper deals with the same structure but the scatterers are illuminated by a plane electromagnetic wave. Following the analytical regularization scheme, one of the present authors developed the singular integral equation method using weighted Chebyshev polynomials as basis functions to the two-dimensional problems of infinite [17] and finite [18] periodic strips in addition to the waveguide diaphragms [19]. Though the array of cylinders that we take up in the present paper has a three-dimensional geometry, the axial symmetry along with the cylindrical wave

Received 14 November 2018, Accepted 10 February 2019, Scheduled 7 March 2019

* Corresponding author: Akira Matsushima (matsua@cs.kumamoto-u.ac.jp).

[1] Graduate School of Science and Technology, Kumamoto University, 2-39-1 Kurokami, Kumamoto 860-8555, Japan. [2] Faculty of Advanced Science and Technology, Kumamoto University, 2-39-1 Kurokami, Kumamoto 860-8555, Japan.

expression of a plane wave permits us to solve two-dimensional problems for radial and axial directions repeatedly for each azimuthal order.

The organization of the paper is as follows. Section 2 is devoted to derive a set of integral equations for the surface current densities, and it is numerically solved by means of the Galerkin method in Section 3. The analytical regularization is introduced in the same section. Section 4 discusses numerical results, in view of convergence, surface current density, scattering cross sections in relation to circular cavity resonance. Hereafter the time factor $e^{j\omega t}$ will be omitted throughout.

2. DERIVATION OF INTEGRAL EQUATIONS

2.1. Formulation of the Problem

As illustrated in Fig. 1(a), an infinite number of hollow circular cylinders with radius a and length w are coaxially arrayed in the z direction with period d in the vacuum of the electric constants ε_0 and μ_0. The cylinders are assumed to be perfectly conducting (PEC) and infinitely thin. The axial symmetry allows us to restrict the wavenumber vector $\mathbf{k}^i$ of an incident plane wave $(\mathbf{E}^i, \mathbf{H}^i)$ to being parallel to the xz plane as shown in Fig. 1(b). This vector is written as $\mathbf{k}^i = -\mathbf{i}_x\beta_0 + \mathbf{i}_z\gamma_0$ with $\beta_0 = k\sin\theta^i$ and $\gamma_0 = k\cos\theta^i$, where $\mathbf{i}_u$ is the u-directed unit vector, $k = \omega\sqrt{\varepsilon_0\mu_0} = 2\pi/\lambda$ a wavenumber, and λ a wavelength. The incident field is given by

$$\mathbf{E}^i(\mathbf{r}) = (\mathbf{i}_x\cos\theta^i\sin\delta^i - \mathbf{i}_y\cos\delta^i + \mathbf{i}_z\sin\theta^i\sin\delta^i)\,e^{-j\mathbf{k}^i\cdot\mathbf{r}}, \quad \mathbf{H}^i(\mathbf{r}) = \mathbf{k}^i\times\mathbf{E}^i(\mathbf{r})/kZ, \tag{1}$$

where $\mathbf{r} = \mathbf{i}_x x + \mathbf{i}_y y + \mathbf{i}_z z = \mathbf{i}_\rho\rho + \mathbf{i}_z z$ is a position vector in the rectangular and cylindrical coordinate systems, and $Z = \sqrt{\mu_0/\varepsilon_0}$ is the wave impedance. The polarization angles $\delta^i = 0$ and $\delta^i = \pi/2$ correspond to the TE- and TM-waves, respectively, regarding to the z axis.

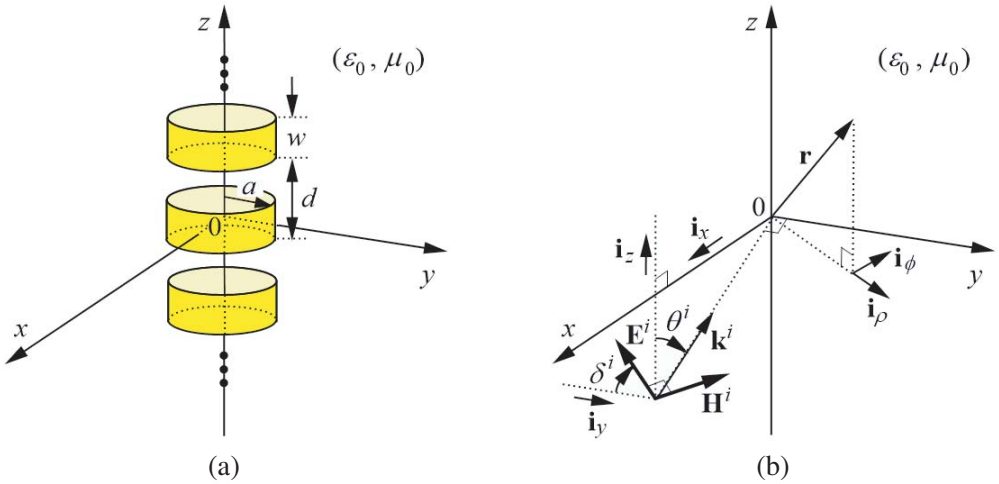

Figure 1. Geometry of the problem. (a) Coaxially periodic array of hollow circular cylinders. (b) An incident plane wave, incidence and polarization angles, and the unit vectors.

Let us decompose the total field as $(\mathbf{E}, \mathbf{H}) = (\mathbf{E}^i, \mathbf{H}^i) + (\mathbf{E}^s, \mathbf{H}^s)$, where the superscript s concerns the unknown scattered field. The periodicity condition $F_u(\mathbf{r} + \mathbf{i}_z d) = e^{-j\gamma_0 d}F_u(\mathbf{r})$ for any field components F_u enables us to deal with one unit cell, say $|z| < d/2$. Taking account of the continuity of $(\mathbf{E}^i, \mathbf{H}^i)$ everywhere, we can express the boundary conditions as

$$\left.\begin{array}{ll} [\mathbf{i}_\rho\times\mathbf{E}^s(\mathbf{r})]_{\rho=a-0}^{\rho=a+0} = 0 & (|z| < d/2), \\ \mathbf{i}_\rho\times\mathbf{E}(\mathbf{r})|_{\rho=a\pm 0} = 0 & (|z| < w/2), \\ \mathbf{J}^s(\phi, z) = 0 & (w/2 < |z| < d/2) \end{array}\right\} \quad (0 \le \phi < 2\pi), \tag{2}$$

where $\mathbf{J}^s(\phi, z) = [\mathbf{i}_\rho\times\mathbf{H}^s(\mathbf{r})]_{\rho=a-0}^{\rho=a+0}$ is the surface current density.

2.2. Expressions of the Field and Current

The Fourier series is an effective tool for separating the variables of electromagnetic fields in the present cylindrical structure. Using the indices m and p in the ϕ and z directions, respectively, we express the u-component of the field F_u $(u = \rho, \phi, z)$ and the surface current density J_u^s $(u = \phi, z)$ as

$$\begin{pmatrix} F_u(\mathbf{r}) \\ J_u^s(\phi, z) \end{pmatrix} = \sum_{m=-\infty}^{\infty} \begin{pmatrix} F_{u,m}(\rho, z) \\ J_{u,m}^s(z) \end{pmatrix} e^{jm\phi}, \quad \begin{pmatrix} F_{u,m}(\rho, z) \\ J_{u,m}^s(z) \end{pmatrix} = \sum_{p=-\infty}^{\infty} \begin{pmatrix} F_{u,mp}(\rho) \\ J_{u,mp}^s \end{pmatrix} e^{-j\gamma_p z}, \tag{3}$$

where $\gamma_p = \gamma_0 + 2p\pi/d$. The scattered field for the outside region $\rho > a$ that satisfies the Helmholtz equation and the radiation condition is expressed as

$$\begin{pmatrix} E_{\rho,mp}^s(\rho) \\ E_{\phi,mp}^s(\rho) \\ E_{z,mp}^s(\rho) \\ ZH_{\rho,mp}^s(\rho) \\ ZH_{\phi,mp}^s(\rho) \\ ZH_{z,mp}^s(\rho) \end{pmatrix} = \begin{pmatrix} (mk/\beta_p^2\rho)H_m^{(2)}(\beta_p\rho) & (\gamma_p/j\beta_p)H_m^{(2)\prime}(\beta_p\rho) \\ (jk/\beta_p)H_m^{(2)\prime}(\beta_p\rho) & (m\gamma_p/\beta_p^2\rho)H_m^{(2)}(\beta_p\rho) \\ 0 & H_m^{(2)}(\beta_p\rho) \\ (\gamma_p/j\beta_p)H_m^{(2)\prime}(\beta_p\rho) & -(mk/\beta_p^2\rho)H_m^{(2)}(\beta_p\rho) \\ (m\gamma_p/\beta_p^2\rho)H_m^{(2)}(\beta_p\rho) & (k/j\beta_p)H_m^{(2)\prime}(\beta_p\rho) \\ H_m^{(2)}(\beta_p\rho) & 0 \end{pmatrix} \begin{pmatrix} J_m'(\beta_p a)A_{1mp} \\ J_m(\beta_p a)A_{2mp} \end{pmatrix}, \tag{4}$$

where $J_m(\cdot)$ and $H_m^{(2)}(\cdot)$ are the Bessel function and Hankel function of the second kind, respectively, and the propagation constant is $\beta_p = (k^2 - \gamma_p^2)^{1/2}$ ($\mathrm{Re}\ \beta_p \geq 0$, $\mathrm{Im}\,\beta_p \leq 0$). The symbols A_{smp} denotes the unknown modal coefficients, where $s = 1$ and $s = 2$ correspond to the TE- and TM-waves, respectively, with respect to z. On the other hand, the field in the inside region $\rho < a$ is written by replacing the functions $(J_m, J_m', H_m^{(2)}, H_m^{(2)\prime})$ in Eq. (4) with $(H_m^{(2)}, H_m^{(2)\prime}, J_m, J_m')$. These expressions, inside and outside the cylinder, automatically satisfy the first condition in Eq. (2), i.e., the continuity of the tangential electric field on the boundary $\rho = a$.

Applying Eq. (4) into the definition of surface current density and using the orthogonality of the functions $e^{j\gamma_p z}$ in the interval $|z| < d/2$, we obtain the relations among the unknowns as

$$A_{1mp} = (j\pi Z\beta_p a/2)\, J_{\phi,mp}^s, \quad A_{2mp} = (-\pi Z\beta_p a/2k)\, \left[(m\gamma_p/\beta_p a)\, J_{\phi,mp}^s + \beta_p J_{z,mp}^s\right] \tag{5}$$

with $J_{u,mp}^s = (1/d)\int_{-w/2}^{w/2} J_{u,m}^s(z)\, e^{j\gamma_p z}\, dz$, in which the range of integration is limited to the cylinder length due to the third condition in Eq. (2), i.e., the absence of current in the vacuum.

With regard to the incident field in Eq. (1), the transformation of a plane wave into an ensemble of cylindrical waves gives

$$\begin{pmatrix} E_{\rho,mp}^i(\rho) \\ E_{\phi,mp}^i(\rho) \\ E_{z,mp}^i(\rho) \\ ZH_{\rho,mp}^i(\rho) \\ ZH_{\phi,mp}^i(\rho) \\ ZH_{z,mp}^i(\rho) \end{pmatrix} = \frac{j^m\beta_0\delta_{p0}}{k} \begin{pmatrix} (mk/\beta_0^2\rho)J_m(\beta_0\rho) & (\gamma_0/j\beta_0)J_m'(\beta_0\rho) \\ (jk/\beta_0)J_m'(\beta_0\rho) & (m\gamma_0/\beta_0^2\rho)J_m(\beta_0\rho) \\ 0 & J_m(\beta_0\rho) \\ (\gamma_0/j\beta_0)J_m'(\beta_0\rho) & -(mk/\beta_0^2\rho)J_m(\beta_0\rho) \\ (m\gamma_0/\beta_0^2\rho)J_m(\beta_0\rho) & (k/j\beta_0)J_m'(\beta_0\rho) \\ J_m(\beta_0\rho) & 0 \end{pmatrix} \begin{pmatrix} \cos\delta^i \\ \sin\delta^i \end{pmatrix}. \tag{6}$$

Here, the appearance of Kronecker's delta δ_{p0} stems from the z dependence $e^{-j\gamma_0 z}$.

2.3. Integral Equations

We have not yet used the second expression of Eq. (2), i.e., the perfect conductor condition. Combining it with Eqs. (3)–(6), we are led to the set of integral equations for the surface current density as

$$2\pi kZ \int_{-w/2}^{w/2} \begin{pmatrix} G_{\phi\phi,m}(z,z') & G_{\phi z,m}(z,z') \\ G_{\phi z,m}(z,z') & G_{zz,m}(z,z') \end{pmatrix} \begin{pmatrix} J_{\phi,m}^s(z') \\ J_{z,m}^s(z') \end{pmatrix} dz' = \begin{pmatrix} E_{\phi,m0}^i(a) \\ E_{z,m0}^i(a) \end{pmatrix} e^{-j\gamma_0 z}$$
$$(|z| < w/2;\ m = 0, \pm 1, \pm 2, \ldots), \tag{7}$$

where the kernel functions are given by

$$\begin{pmatrix} G_{\phi\phi,m}(z,z') \\ G_{\phi z,m}(z,z') \\ G_{zz,m}(z,z') \end{pmatrix} = \frac{a}{4d} \sum_{p=-\infty}^{\infty} \begin{pmatrix} C_{\phi\phi,mp} \\ (m/k^2a^2)C_{\phi z,mp} \\ (1/k^2a^2)C_{zz,mp} \end{pmatrix} e^{-j\gamma_p(z-z')} \tag{8}$$

with

$$\begin{cases} C_{\phi\phi,mp} = J'_m(\beta_p a)H_m^{(2)\prime}(\beta_p a) + (m\gamma_p/k\beta_p a)^2 J_m(\beta_p a)H_m^{(2)}(\beta_p a), \\ C_{\phi z,mp} = \gamma_p a J_m(\beta_p a)H_m^{(2)}(\beta_p a), \\ C_{zz,mp} = \beta_p^2 a^2 J_m(\beta_p a)H_m^{(2)}(\beta_p a). \end{cases} \tag{9}$$

3. NUMERICAL ANALYSIS

3.1. Galerkin's Method

Let us solve the integral equations (7) numerically by means of the Galerkin method that is one version of the method of moments [8]. Taking account of the behavior of surface current density near the conductor edges, we express the unknown functions in terms of the expansion coefficients $f_{u,mn'}$ $(u = \phi, m)$ as

$$\begin{pmatrix} J^s_{\phi,m}(z) \\ J^s_{z,m}(z) \end{pmatrix} \approx \frac{1}{2\pi^2 Z} \sum_{n'=0}^{\infty} j^{-n'} \begin{pmatrix} f_{\phi,mn'}\,\tilde{T}_{n'}(2z/w) \\ f_{z,mn'}\,\tilde{U}_{n'}(2z/w) \end{pmatrix} e^{-j\gamma_0 z} \quad (|z| < w/2;\ m = 0, \pm1, \pm2, \ldots), \tag{10}$$

where the basis functions

$$\tilde{T}_n(\zeta) = T_n(\zeta)/\sqrt{1-\zeta^2}, \quad \tilde{U}_n(\zeta) = \sqrt{1-\zeta^2}\,U_n(\zeta)/(n+1) \tag{11}$$

are the weighted forms of the Chebyshev polynomials of the first kind $T_n(\cdot)$ and second kind $U_n(\cdot)$.

We substitute Eq. (10) into Eq. (7), multiply the upper and lower expressions by $(j^n/\pi w)\,\tilde{T}_n(2z/w)\,e^{j\gamma_0 z}$ and $(j^n/\pi w)\,\tilde{U}_n(2z/w)\,e^{j\gamma_0 z}$ $(n = 0, 1, \ldots)$, respectively, and integrate them from $z = -w/2$ to $w/2$. This procedure leads us to the set of simultaneous linear equations as

$$\sum_{n'=0}^{\infty} \begin{pmatrix} G_{\phi\phi,mnn'} & G_{\phi z,mnn'} \\ G_{\phi z,mn'n} & G_{zz,mnn'} \end{pmatrix} \begin{pmatrix} f_{\phi,mn'} \\ f_{z,mn'} \end{pmatrix} = \begin{pmatrix} E^i_{\phi,mn} \\ E^i_{z,mn} \end{pmatrix} \quad (n = 0, 1, \ldots;\ m = 0, \pm1, \pm2, \ldots), \tag{12}$$

where the system and excitation elements are given by the double and single integrals, respectively, as

$$\begin{pmatrix} G_{\phi\phi,mnn'} \\ G_{\phi z,mnn'} \\ G_{zz,mnn'} \end{pmatrix} = \frac{j^{n-n'}k}{\pi^2 w} \int_{-w/2}^{w/2}\int_{-w/2}^{w/2} \begin{pmatrix} \tilde{T}_n(2z/w)\,\tilde{T}_{n'}(2z'/w)\,G_{\phi\phi,m}(z,z') \\ \tilde{T}_n(2z/w)\,\tilde{U}_{n'}(2z'/w)\,G_{\phi z,m}(z,z') \\ \tilde{U}_n(2z/w)\,\tilde{U}_{n'}(2z'/w)\,G_{zz,m}(z,z') \end{pmatrix} e^{j\gamma_0(z-z')}\,dz'\,dz \tag{13}$$

and

$$\begin{pmatrix} E^i_{\phi,mn} \\ E^i_{z,mn} \end{pmatrix} = \frac{j^n}{\pi w} \int_{-w/2}^{w/2} \begin{pmatrix} \tilde{T}_n(2z/w)\,E^i_{\phi,m0}(a) \\ \tilde{U}_n(2z/w)\,E^i_{z,m0}(a) \end{pmatrix} dz. \tag{14}$$

In order to evaluate the integrals in Eqs. (13) and (14), we normalize the range of integration by $z = wt/2$ and make use of the formulas

$$\int_{-1}^{1} \tilde{T}_n(t)\,e^{-j\zeta t}\,dt = \pi j^{-n} J_n(\zeta), \quad \int_{-1}^{1} \tilde{U}_n(t)\,e^{-j\zeta t}\,dt = \frac{\pi j^{-n}}{\zeta}\,J_{n+1}(\zeta) \tag{15}$$

with limiting procedures $J_n(\zeta) \to \delta_{n0}$ and $J_{n+1}(\zeta)/\zeta \to \delta_{n0}/2$ as $\zeta \to 0$. At first, combination of Eqs. (14), (15), and (6) gives

$$\begin{pmatrix} E^i_{\phi,mn} \\ E^i_{z,mn} \end{pmatrix} = \frac{j^m \delta_{n0}}{2} \begin{pmatrix} jJ'_m(\beta_0 a) & (m\gamma_0/k\beta_0 a)J_m(\beta_0 a) \\ 0 & (\beta_0/2k)J_m(\beta_0 a) \end{pmatrix} \begin{pmatrix} \cos\delta^i \\ \sin\delta^i \end{pmatrix}. \tag{16}$$

On the other hand, though Eq. (13) could be handled in a similar manner by using Eq. (15), such straightforward treatment spoils the numerical stability while solving Eq. (12). This is caused by the singularities originating from the infinite sums in Eq. (8) as $z \to z'$, and is called the relative convergence

phenomenon [20]. We will overcome this difficulty by means of the analytical regularization in the next subsection.

Solving Eq. (12) numerically by retaining $0 \le n' \le N$, $0 \le n \le N$ and $-M \le m \le M$, we can obtain the surface current density by Eq. (10). Application of this result into Eq. (5) leads us to the modal coefficients as

$$\begin{cases} A_{1mp} = \dfrac{j\beta_p aw}{8d} \displaystyle\sum_{n=0}^{\infty} f_{\phi,mn} J_n\left(\frac{p\pi w}{d}\right), \\ A_{2mp} = -\dfrac{1}{8kd}\left[m\gamma_p w \displaystyle\sum_{n=0}^{\infty} f_{\phi,mn} J_n\left(\frac{p\pi w}{d}\right) + \frac{\beta_p^2 ad}{p\pi} \sum_{n=0}^{\infty} f_{z,mn} J_{n+1}\left(\frac{p\pi w}{d}\right)\right]. \end{cases} \tag{17}$$

3.2. Analytical Regularization

Let us extract the singularities from the elements in Eq. (13) and separate them into the dominant and compensative parts, the former of which includes Kronecker's delta $\delta_{nn'}$. This procedure modifies the set of equations (12) into the form of Fredholm second kind, and makes the numerical solution stable and convergent.

Taking into account the behavior of the propagation constants and cylindrical functions in Eq. (9) as $|p| \to \infty$, we define the modified coefficients by subtracting the asymptotic parts as

$$\left.\begin{array}{l} \tilde{C}_{\phi\phi,mp} = C_{\phi\phi,mp} - j\kappa_m d/2|p|\pi^2 a, \\ \tilde{C}_{\phi z,mp} = C_{\phi z,mp} - j\,\mathrm{sgn}(p)/\pi, \\ \tilde{C}_{zz,mp} = C_{zz,mp} - 2|p|a/jd \end{array}\right\} \quad (p \ne 0), \qquad \left.\begin{array}{l} \tilde{C}_{\phi\phi,mp} = 0(p^{-2}), \\ \tilde{C}_{\phi z,mp} = 0(p^{-2}), \\ \tilde{C}_{zz,mp} = 0(p^{0}) \end{array}\right\} \quad (|p| \to \infty) \tag{18}$$

with $\kappa_m = 1 - (m/ka)^2$. With the aid of Eq. (18), the infinite sums in Eq. (8) are decomposed into two types of sums. The first type is written in terms of $\tilde{C}_{\phi\phi,mp}$, $\tilde{C}_{\phi z,mp}$, and $\tilde{C}_{zz,mp}$, and the convergence of these sums is accelerated compared with the original ones in Eq. (8). The second type, with regard to the second terms in the right hand side of Eq. (18), is analytically evaluated by using the formulas

$$\sum_{\substack{p=-\infty \\ (p\ne 0)}}^{\infty} \begin{pmatrix} 1/|p| \\ \mathrm{sgn}(p) \\ |p| \end{pmatrix} e^{-jp\zeta} = \begin{pmatrix} -2\log[2\sin(|\zeta|/2)] \\ -j\cot(\zeta/2) \\ -(1/2)\csc^2(\zeta/2) \end{pmatrix} \sim \begin{pmatrix} -2\log|\zeta| \\ 2/j\zeta \\ -2/\zeta^2 - 1/6 \end{pmatrix} \quad (\zeta \to 0). \tag{19}$$

Note that the sums with respect to $\mathrm{sgn}(p)e^{-jp\zeta}$ and $|p|e^{-jp\zeta}$ hold in the sense of distributions. As a result, the elements in Eq. (13) are decomposed as

$$\begin{cases} G_{\phi\phi,mnn'} = \dfrac{j^{n-n'}kaw}{16\pi^2 d} \displaystyle\int_{-1}^{1}\int_{-1}^{1} \left[\frac{\kappa_m d}{j\pi^2 a}\log|t-t'| + C_{\phi\phi,m0} + \sum_{\substack{p=-\infty \\ (p\ne 0)}}^{\infty} \tilde{C}_{\phi\phi,mp}\, e^{-jp\pi w(t-t')/d} \right. \\ \qquad \left. + \dfrac{\kappa_m d}{j\pi^2 a} F_{\phi\phi}(t-t')\right] \tilde{T}_n(t)\,\tilde{T}_{n'}(t')\,dt'\,dt, \\ G_{\phi z,mnn'} = \dfrac{mj^{n-n'}w}{16\pi^2 kad} \displaystyle\int_{-1}^{1}\int_{-1}^{1} \left[\frac{2d}{\pi^2 w(t-t')} + C_{\phi z,m0} + \sum_{\substack{p=-\infty \\ (p\ne 0)}}^{\infty} \tilde{C}_{\phi z,mp}\, e^{-jp\pi w(t-t')/d} \right. \\ \qquad \left. + \dfrac{1}{\pi} F_{\phi z}(t-t')\right] \tilde{T}_n(t)\,\tilde{U}_{n'}(t')\,dt'\,dt, \\ G_{zz,mnn'} = \dfrac{j^{n-n'}w}{16\pi^2 kad} \displaystyle\int_{-1}^{1}\int_{-1}^{1} \left[\frac{j4ad}{\pi^2 w^2(t-t')^2} + C_{zz,m0} + \sum_{\substack{p=-\infty \\ (p\ne 0)}}^{\infty} \tilde{C}_{zz,mp}\, e^{-jp\pi w(t-t')/d} \right. \\ \qquad \left. + \dfrac{ja}{d} F_{zz}(t-t')\right] \tilde{U}_n(t)\,\tilde{U}_{n'}(t')\;dt'\,dt, \end{cases} \tag{20}$$

where we introduced the singularity-free functions as

$$F_{\phi\phi}(t) = \log\left(\frac{2}{t}\,\sin\frac{\pi w t}{2d}\right), \quad F_{\phi z}(t) = \cot\frac{\pi w t}{2d} - \frac{2d}{\pi w t}, \quad F_{zz}(t) = \csc^2\frac{\pi w t}{2d} - \frac{4d^2}{\pi^2 w^2 t^2}. \tag{21}$$

The double integrals in Eq. (20), from term to term, are evaluated as follows.

- Regarding the logarithmic and Cauchy type singularities and the hypersingularity, analytical treatment is given by making use of the formulas

$$\begin{cases} \displaystyle\int_{-1}^{1}\int_{-1}^{1} \tilde{T}_n(t)\,\tilde{T}_{n'}(t')\,\log|t-t'|\,dt'\,dt = -\pi^2\delta_{nn'} \times \begin{cases} \log 2 & (n=0) \\ 1/2n' & (n=1,2,\ldots) \end{cases}, \\ \displaystyle\int_{-1}^{1}\int_{-1}^{1} \frac{\tilde{T}_n(t)\,\tilde{U}_{n'}(t')}{t-t'}\,dt'\,dt = \frac{\pi^2\delta_{n\,n'+1}}{2(n'+1)}, \\ \displaystyle\int_{-1}^{1}\int_{-1}^{1} \frac{\tilde{U}_n(t)\,\tilde{U}_{n'}(t')}{(t-t')^2}\,dt'\,dt = -\frac{\pi^2}{2(n'+1)}\,\delta_{nn'}. \end{cases} \tag{22}$$

  The appearance of Kronecker's delta is of considerable merit which contributes to the stability and convergence of the numerical solution of Eq. (12).

- The integrals concerning $e^{-jp\pi w(t-t')/d}$ are analytically evaluated by using Eq. (15) and expressed in terms of the Bessel functions, say $J_n(p\pi w/d)$. The limiting procedure is applied for $p=0$. The terms for $-P \le p \le P$ are retained in the numerical computation.

- The functions in Eq. (21) are finite and smooth even when $t \to 0$, and thereby accurately integrated by means of the quadrature formulas of the Gauss-Chebyshev type with L nodes as

$$\begin{cases} \displaystyle\int_{-1}^{1} \frac{F(t)}{\sqrt{1-t^2}}\,dt \approx \frac{\pi}{L}\sum_{l=1}^{L} F\left(\cos\frac{(2l-1)\pi}{2L}\right), \\ \displaystyle\int_{-1}^{1} \sqrt{1-t^2}\,F(t)\,dt \approx \frac{\pi}{L+1}\sum_{l=1}^{L} \sin^2\frac{l\pi}{L+1}\,F\left(\cos\frac{l\pi}{L+1}\right). \end{cases} \tag{23}$$

3.3. Scattering and Extinction Cross Sections

The total scattering cross section per unit region σ^t is defined by dividing the radiated power $(1/2)\,\mathrm{Re}\{\int_{-d/2}^{d/2}\int_{-\pi}^{\pi}\,[\mathbf{E}^s(\mathbf{r}) \times \mathbf{H}^{s*}(\mathbf{r})]_{\rho>a} \cdot \mathbf{i}_\rho\,\rho\,d\phi\,dz\}$ by the incident power density $W^i = 1/2Z$. By using Eq. (4) and carrying out the integrations, the result is arranged in the form

$$\sigma^t = \sum_{\substack{p \\ (\mathrm{Re}\,\beta_p>0)}} \left(\sigma_p^{\mathrm{TE}} + \sigma_p^{\mathrm{TM}}\right), \tag{24}$$

where the modal scattering cross sections are computed by

$$\begin{pmatrix} \sigma_p^{\mathrm{TE}} \\ \sigma_p^{\mathrm{TM}} \end{pmatrix} = \frac{4kd}{\beta_p^2} \sum_{m=-\infty}^{\infty} \begin{pmatrix} J_m'^2(\beta_p a)|A_{1mp}|^2 \\ J_m^2(\beta_p a)|A_{2mp}|^2 \end{pmatrix}. \tag{25}$$

The power conservation is expressed by $\mathrm{Re}\{\int_{-d/2}^{d/2}\int_{-\pi}^{\pi}\,[\mathbf{E}(\mathbf{r}) \times \mathbf{H}^*(\mathbf{r})]_{\rho>a} \cdot \mathbf{i}_\rho\,\rho\,d\phi\,dz\} = 0$. Taking account of the fact that the integral with respect to $\mathbf{E}^i(\mathbf{r}) \times \mathbf{H}^{i*}(\mathbf{r})$ vanishes, we obtain the optical theorem $\sigma^t = \sigma^e$, where the extinction cross section is given by

$$\begin{aligned} \sigma^e &= -\frac{1}{2W^i}\,\mathrm{Re}\left(\int_{\phi=-\pi}^{\pi}\int_{z=-d/2}^{d/2} \left\{\left[\mathbf{E}^i(\mathbf{r}) \times \mathbf{H}^{s*}(\mathbf{r})\right] + \left[\mathbf{E}^s(\mathbf{r}) \times \mathbf{H}^{i*}(\mathbf{r})\right]\right\}_{\rho>a} \cdot \mathbf{i}_\rho\,\rho\,d\phi\,dz\right) \\ &= -\frac{4d}{\beta_0}\,\mathrm{Re}\left\{\sum_{m=-\infty}^{\infty}\left[J_m'(\beta_0 a)A_{1m0}\cos\delta^i + J_m(\beta_0 a)A_{2m0}\sin\delta^i\right]\right\}. \end{aligned} \tag{26}$$

4. NUMERICAL RESULTS

4.1. Convergence

Numerical computations were carried out by making a Fortran code with the aid of the libraries for special functions and LU decomposition. We have introduced four truncation numbers N, M, P, and L, which must be appropriately chosen in order to yield convergent results. The numbers except N are determined in the following way.

- The number M is fixed at $M \approx 9 + 1.07\,ka - 16/(2 + ka)$ $(0 \leq ka \leq 100)$, which is noted as Eq. (12) in Ref. [21] as the 0.1%-error criterion. This is based on the Debye asymptotic expansion of cylindrical functions which appears in the scattering problems with regard to cylinders.
- Combination of Eqs. (15) and (18) tells us that the double integrals concerning $(\tilde{C}_{\phi\phi,mp}\tilde{T}_n(t)\tilde{T}_{n'}(t'),\ \tilde{C}_{\phi z,mp}\tilde{T}_n(t)\tilde{U}_{n'}(t'),\ \tilde{C}_{zz,mp}\tilde{U}_n(t)\tilde{U}_{n'}(t')) \times e^{-jp\pi w(t-t')/d}$ in (20) behave as $O(p^{-3})$ as $|p| \to \infty$. Taking account that $|\sum_{p=1}^{32} p^{-3}/\sum_{p=1}^{\infty} p^{-3}| = 0.99961$, we can reasonably set as $P = 32$ on the permission of 0.04%-error.
- Owing to both the analytical view and numerical experiment, number L is selected as $L = [N/2]+4$, where $[\zeta]$ is the largest integer not exceeding ζ. In fact, the quadrature formulas in Eq. (23) yield exact values if the function $F(t)$ is a polynomial of the order $2L-1$ or less. The bias "+4" is added by considering that the functions $F_{\phi\phi}(t)$, $F_{\phi z}(t)$, and $F_{zz}(t)$ in Eq. (21) are not finite polynomials but in the class C^{∞}.

Figure 2 shows the logarithmic plot of errors in the total scattering cross sections computed from Eqs. (24), (25), and (17) as functions of the truncation number N. The values w/λ and P are selected in two ways, and the other truncation numbers M and L are determined in the manner mentioned in the previous paragraph. The error curves are, except some dips due to the overshoot, decreased on the whole as N increases, which tells that the relative convergence is avoided. The errors saturate for $N \geq 12$ since M and P are fixed: for larger M and P the error would begin to saturate at larger N. As expected, the decrement of errors is faster for the shorter cylinder ($w = 0.5\lambda$) and the larger truncation number ($P = 32$). There is no appreciable difference in the degree of errors between TE- and TM-incidences. Note that the error on the optical theorem defined by $\varepsilon^{opt} = 2\,|\sigma^t - \sigma^e|/|\sigma^t + \sigma^e|$ is always satisfied on the machine epsilon level, i.e., less than 10^{-15} at double precision processing [22].

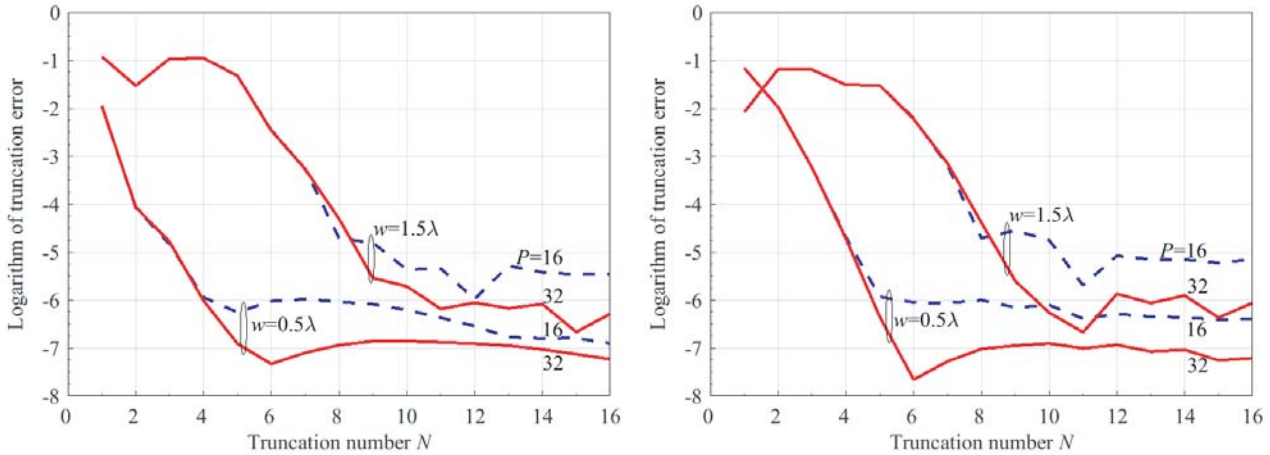

Figure 2. Normalized truncation errors $\log_{10}|\sigma^t(N)/\sigma^t(2N)-1|$ as functions of the truncation number N. The parameters are $a = 0.5\lambda$, $w/d = 0.5$, $\theta^i = 45°$, $M = 9$, and $L = [N/2] + 4$. (a) TE-incidence $\delta^i = 0°$; (b) TM-incidence $\delta^i = 90°$.

4.2. Surface Current Density

Figure 3 shows the amplitude of the surface current density normalized by the incident magnetic field strength for three different values of the period d, where the radius a and the length w are fixed at one wavelength. The computation is based on Eq. (10) after solving the simultaneous equations (12). The observation point moves along the line segment on the illuminated side $\rho = a$ and $\phi = 0$. For TE- and TM-incidences, the dominant ϕ and z components are depicted, respectively, which exhibit appropriate edge behaviors thanks to the weighting factors $[1-(2z/w)^2]^{\mp 1/2}$. The z component in Fig. 3(b) resemble a standing wave having two loops with an average value 2 corresponding to the physical optics current. For a suggestive confirmation, we appended the curves for an isolated cylinder [7] marked as $d \to \infty$. As the period d is increased, meaning that adjacent cylinders move away, the curve gradually approaches the one for the isolated case.

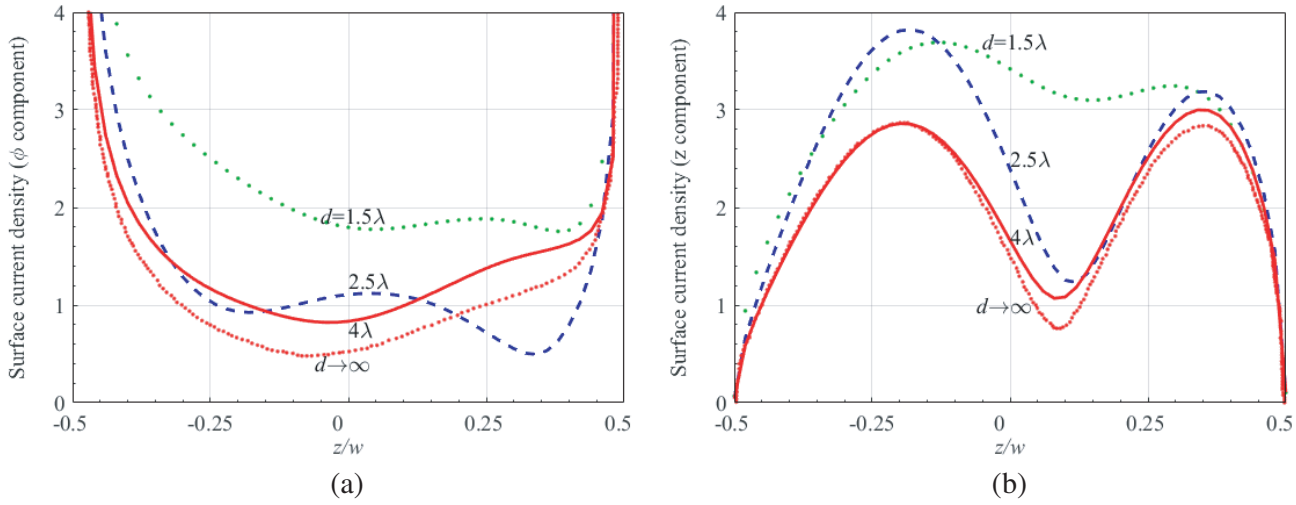

Figure 3. Amplitude of the normalized surface current density $|J_u^s(0,z)|/|\mathbf{H}^i|$ $(u = \phi, z)$ observed along the line segment joining two edge points $(\rho, \phi, z) = (a, 0, \pm w/2)$. The parameters are $a = w = \lambda$ and $\theta^i = 45°$. The description $d \to \infty$ means an isolated cylinder, the data for which is taken from Fig. 3 of [7]. (a) ϕ component at TE-incidence $\delta^i = 0°$; (b) z component at TM-incidence $\delta^i = 90°$.

4.3. Scattering Cross Section

From the viewpoint of far field, we show in Fig. 4 the modal scattering cross sections computed from Eqs. (24), (25), and (17) normalized by the rectangular area composed of the period d and the diameter $2a$. At normal incidence where $\theta^i = 90°$, the cutoff wavelengths for the 0th, $\pm$1st, and $\pm$2nd order modes correspond to $d/\lambda = 0$, 1, and 2, respectively. Emerging higher order mode causes the abrupt change in the curve for lower order mode, which is called Wood's anomaly [23]. Generally speaking, the co-polarization in solid curves is stronger than the cross-polarization in dotted ones: the exception is the range $1.7 < d/\lambda < 2$ in Fig. 4(a).

Figure 5 shows the normalized scattering cross sections for each mode as functions of normalized radius of cylinders at both TE- and TM-incidences. At $d = 1.5\lambda$ and $\theta^i = 90°$, the grating modes of the dominant 0th order and the degenerated higher $\pm$1st orders are propagating. All the curves repeat peaks and dips at uneven intervals as a/λ changes. This phenomenon is examined in detail by taking account of the excited circular waveguide modes: each cylinder play a role of an open type circular resonator. The data for the cutoff wavelengths given in Table 1 help us to interpret the points of appearance of resonances. Such points nearly agree with $TM_{01,11}$ waveguide modes in Fig. 5(b) (the inset marks a and b), whereas the resonances seen in Fig. 5(a) (the inset marks a, b, c, d, e, and f) are a little shifted from the cutoff of $TE_{11,21,01,31}$ modes. This discord is due to the formation of different cavity modes, which will be discussed in the next subsection in view of the near fields. Note that the curves for 0th

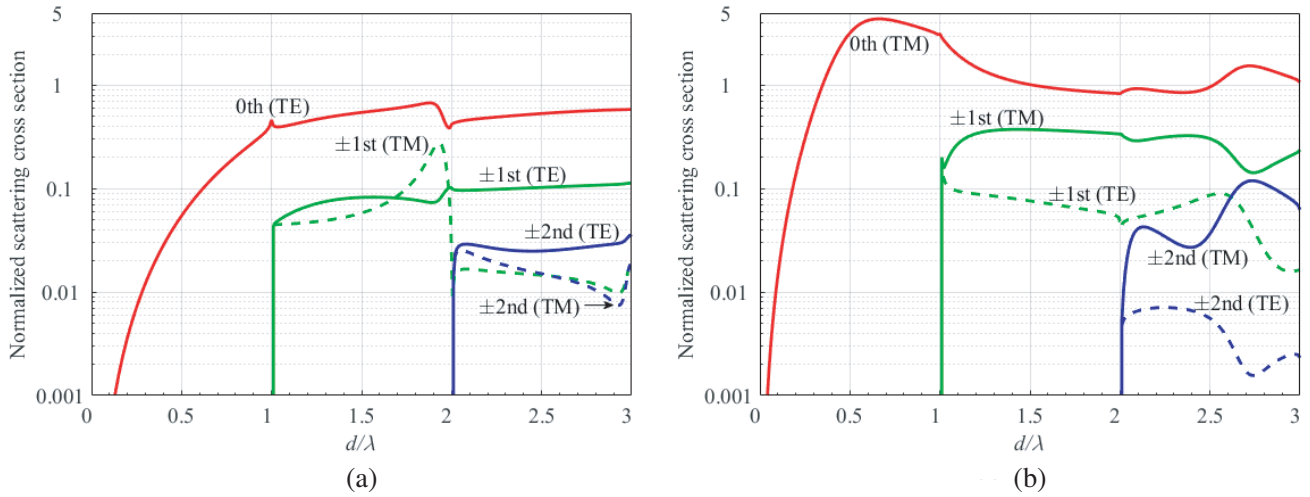

Figure 4. Normalized modal scattering cross sections $\sigma_p^{\mathrm{TE,TM}}/2ad$ $(p = 0, \pm 1, \pm 2)$ as functions of d/λ. The parameters are $a/d = 0.1$, $w/d = 0.6$, and $\theta^i = 90°$. (a) TE-incidence $\delta^i = 0°$; (b) TM-incidence $\delta^i = 90°$.

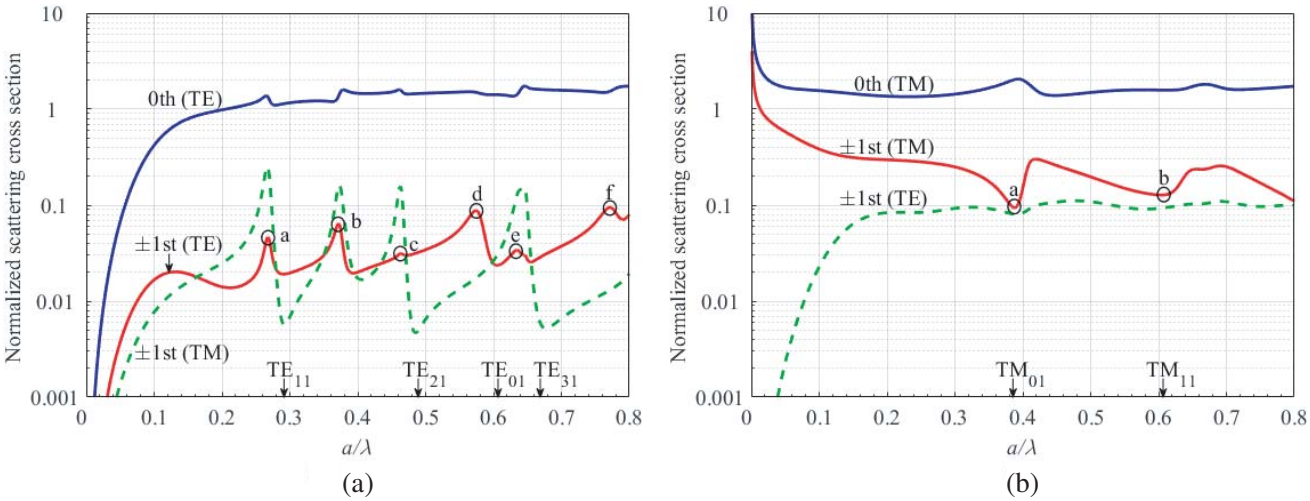

Figure 5. Normalized mode scattering cross sections $\sigma_p^{\mathrm{TE,TM}}/2ad$ $(p = 0, \pm 1)$ as functions of a/λ. The parameters are $d = 1.5\lambda$, $w/d = 0.75$, and $\theta^i = 90°$. The arrows pointing to abscissas denote the cutoff of circular waveguide modes presented in Table 1. (a) TE-incidence $\delta^i = 0°$; (b) TM-incidence $\delta^i = 90°$.

Table 1. Data for the cutoff of circular waveguide modes. Zeros relating to the Bessel function are such that $J'_m(\xi'_{mn}) = 0$ and $J_m(\xi_{mn}) = 0$ for TE_{mn} and TM_{mn} modes, respectively. The ratio of radius to cutoff wavelength is given by $a/\lambda_{c,mn} = \xi'_{mn}/2\pi$ $(\xi_{mn}/2\pi)$.

Waveguide mode	TE_{11}	TE_{21}	TE_{01}	TE_{31}	TM_{01}	TM_{11}
ξ'_{mn} (ξ_{mn})	1.841	3.054	3.832	4.201	2.405	3.832
$a/\lambda_{c,mn}$	0.293	0.486	0.610	0.669	0.383	0.610

(TM) and ±1st (TM) modes in Fig. 5(b) behave as $O((a/\lambda)^{-1/2})$ in the limit $a/\lambda \to 0$. This means that the scattering cross section $\sigma^{TM}_{0,\pm1}$ itself diminishes in the order of $a^{1/2}$ for thin cylinders.

4.4. Near Field Distribution at Resonance

Figure 6 shows the time averaged amplitude of the axial total magnetic field component which was computed from Eqs. (4), (6), and (17) after solving the simultaneous equations (12). Six values of a/λ are chosen from the resonant points in Fig. 5(a) at TE-incidence, where we observe waveguide mode-like patterns inside the circular cross section regions. The PEC boundary condition states that the magnetic field shows no variation in the radial direction on the cylindrical surface, which we can roughly see from the images. In order to examine the resonance quantitatively, we recall that the resonant wavelength of a circular resonator is given by (See, e.g., Eq. (6.53) of Ref. [24])

$$\frac{a}{\lambda_{r,mn\ell}} = \sqrt{\left(\frac{a}{\lambda_{c,mn}}\right)^2 + \left(\frac{\ell a}{2w}\right)^2}. \tag{27}$$

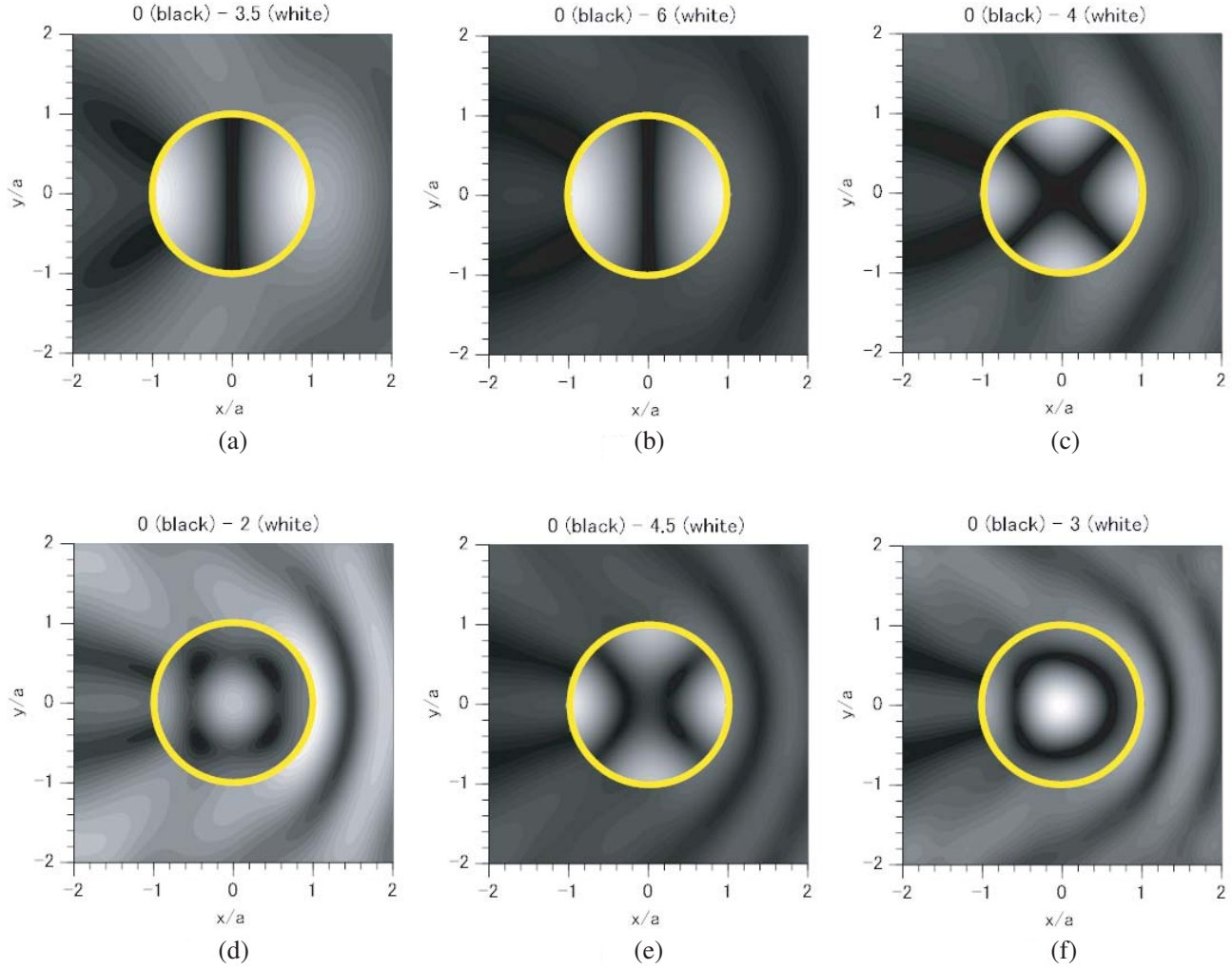

Figure 6. Amplitude of the axial total magnetic field normalized by the incident one on the xy-plane, $|H_z(x, y, 0)|/|\mathbf{H}^i|$, at TE-incidence. The parameters are the same as those in Fig. 5(a). The range of amplitude is written as "0 (black) — maximum (white)" on the top of each map. (a) $a = 0.268\lambda$; (b) $a = 0.372\lambda$; (c) $a = 0.464\lambda$; (d) $a = 0.574\lambda$; (e) $a = 0.635\lambda$; (f) $a = 0.772\lambda$.

Table 2. Resonant points in Fig. 5 and corresponding circular cavity modes.

Inset marks in Fig. 5(a)|(b)	a	b	c	d	e	f	a	b
Cavity modes	TE_{110}	TE_{111}	TE_{210}	TE_{010}	TE_{211}	TE_{011}	TM_{010}	TM_{110}
a/λ in Fig. 5	0.268	0.372	0.464	0.574	0.635	0.772	0.388	0.604
$a/\lambda_{r,nm\ell}$ from Eq. (27)	0.293	0.327	0.486	0.610	0.542	0.680	0.383	0.610
Shift: $\lvert 1-\lambda/\lambda_{r,nm\ell}\rvert$	9%	12%	5%	6%	15%	12%	1%	1%

Applying $\ell = 1$, $d \approx 1.5\lambda_{r,mn1}$, and $w/d = 0.75$ into Eq. (27), we obtain $a/\lambda_{r,mn1} \approx 1.116(a/\lambda_{c,mm})$. These resonance data, as well as the names of configured cavity modes, are gathered in Table 2. The relative shifts from the theoretical $\lambda_{r,nm\ell}$ toward the actual λ are at most 9% and 15% for $\ell = 0$ and $\ell = 1$, respectively. Though this discrepancy is not so small due to the end effect and low Q-factor of the cylinders, the above interpretation is helpful in comprehending the resonance properties.

Figure 7 was drawn in a similar fashion as Fig. 6 by replacing the electric field with the magnetic one in order to study Fig. 5(b). Two resonant values of a/λ are selected. We easily observe that the axial electric field almost vanishes as depicted in black on the surface of a cylinder, that is, the PEC boundary condition is satisfied. As shown in Table 2, the resonant wavelength λ is confidently anticipated by using that of a circular cavity $\lambda_{r,n10}$ with only 1%-shift. This advantage is probably because the axial current flow urges the electromagnetic field to be localized inside the cylinder.

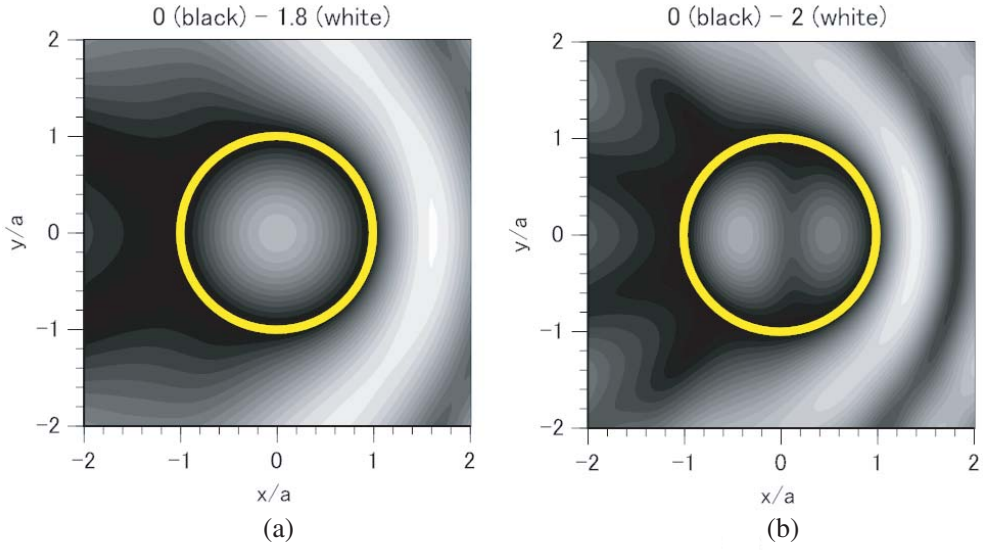

Figure 7. Amplitude of the axial total electric field normalized by the incident one on the xy-plane, $|E_z(x, y, 0)|/|\mathbf{E}^i|$, at TM-incidence. The parameters are the same as those in Fig. 5(b). (a) $a = 0.388\lambda$; (b) $a = 0.604\lambda$.

5. CONCLUSION

A powerful numerical solution has been demonstrated for the scattering of electromagnetic waves from an infinite periodic array of perfectly conducting cylinders of finite length. The boundary value problem is reduced to a set of integral equations for induced surface current density functions. The Galerkin method is employed to lead simultaneous linear equations for expansion coefficients of the current densities in terms of Chebyshev polynomials with weighting factors corresponding to the edge conditions. To attain the stability and fast convergence in the numerical processing, we apply the analytical regularization to the matrix elements. Verifying the far and near fields, we relate the abrupt changes in scattering cross section with the waveguide mode resonances.

The present work was limited to treating perfectly conducting scatterers; however, the extension of the material into metals, semiconductors, dielectric silver is much more interesting [25, 26] since another type of resonance is expected due to the effect of conductivity. Among them, noble metals such as gold and silver are the object of plasmonics in the visual light range, and the factor of resonance thereat is not only the periodicity and cavity geometry but also the excited plasmon surface waves. The use of impedance type boundary conditions [27] enables us to solve the problem of noble metal cylinders as done for periodically allocated disks [28]. This content will be reported in the near future.

ACKNOWLEDGMENT

The authors express hearty thanks to Mr. Daichi Yahata of Kumamoto University for his assistance in numerical computations.

REFERENCES

1. Williams, W. E., "Diffraction by a cylinder of finite length," *Proc. Camb. Phil. Soc.*, Vol. 52, No. 2, 322–335, 1956.
2. Aoki, K., "Diffraction of plane electromagnetic waves from a conductive circular cylinder of finite length," *J. IECE*, Vol. 44, No. 9, 51–56, 1961 (in Japanese).
3. Kinoshita, T. and T. Sekiguchi, "Scattering of a plane electromagnetic wave by a conducting circular cylinder of finite length," *Electron. Commun. Jpn. (Part I)*, Vol. 64, No. 5, 80–88, 1981.
4. Kao, C. C., "Three-dimensional electromagnetic scattering from a circular tube of finite length," *J. Appl. Phys.*, Vol. 40, No. 12, 4732–4740, 1969.
5. Medgyesi-Mitschang, L. N. and C. Eftimiu, "Scattering from wires and open circular cylinders of finite length using entire domain Galerkin expansions," *IEEE Trans. Antennas Propag.*, Vol. 30, No. 4, 628–636, 1982.
6. Davis, A. M. J. and R. W. Scharstein, "Electromagnetic plane wave excitation of an open-ended, finite-length conducting cylinder," *Journal of Electromagnetic Waves and Applications*, Vol. 7, No. 2, 301–319, 1993.
7. Lucido, M., M. D. Migliore, and D. Pinchera, "A new analytically regularizing method for the analysis of the scattering by a hollow finite-length PEC circular cylinder," *Progress In Electromagnetics Research B*, Vol. 70, 55–71, 2016.
8. Harrington, R. F., *Field Computation by Moment Methods*, Macmillan, New York, 1968.
9. Nosich, A. I., "Method of analytical regularization in computational photonics," *Radio Sci.*, Vol. 51, No. 8, 1421–1430, 2016.
10. Freni, A., C. Mias, and R. L. Ferrari, "Hybrid finite-element analysis of electromagnetic plane wave scattering from axially periodic cylindrical structures," *IEEE Trans. Antennas Propagat.*, Vol. 46, No. 12, 1859–1866, 1998.
11. Kishk, A. A., P.-S. Kildal, A. Monorchio, and G. Manara, "Asymptotic boundary condition for corrugated surfaces, and its application to scattering from circular cylinders with dielectric filled corrugations," *IEE Proc. Microw. Antennas Propagat.*, Vol. 145, No. 1, 116–122, 1998.
12. Kishk, A. A., "Electromagnetic scattering from transversely corrugated cylindrical structures using the asymptotic corrugated boundary conditions," *IEEE Trans. Antennas Propagat.*, Vol. 52, No. 11, 3104–3108, 2004.
13. Dincer, F., M. Karaaslan, S. Colak, E. Tetik, O. Akgol, O. Altıntas, and C. Sabah, "Multi-band polarization independent cylindrical metamaterial absorber and sensor application," *Modern Physics Letters B*, Vol. 30, No. 8, 1650095, 2016.
14. Bakir, M., M. Karaaslan, O. Akgol, O. Altıntas, E. Unal, and C. Sabah, "Sensory applications of resonator based metamaterial absorber," *Optik*, Vol. 168, 741–746, 2018.
15. Alkurt, F. O., O. Altıntas, A. Atci, M. Bakir, E. Unal, O. Akgol, K. Delihacioglu, M. Karaaslan, and C. Sabah, "Antenna-based microwave absorber for imaging in the frequencies of 1.8, 2.45, and 5.8 GHz," *Optical Engineering*, Vol. 57, No. 11, 113102, 2018.

16. Agranovich, Z. S. and V. P. Shestopalov, "Distribution of electromagnetic waves in a circular waveguide," *Soviet Phys. — Tech. Phys.*, Vol. 9, No. 11, 1504–1511, 1965.
17. Zinenko, T. L., A. Matsushima, and A. I. Nosich, "Surface-plasmon, grating-mode, and slab-mode Resonances in the H- and E-polarized THz wave scattering by a graphene strip grating embedded into a dielectric slab," *IEEE J. Selected Topics in Quantum Electronics*, Vol. 23, No. 4, 4601809, 2017.
18. Matsushima, A. and T. Itakura, "Singular integral equation approach to electromagnetic scattering from a finite periodic array of conducting strips," *Journal of Electromagnetic Waves and Applications*, Vol. 5, No. 6, 545–562, 1991.
19. Matsushima, A. and T. Itakura, "Accurate numerical analysis of inductive windows in a rectangular waveguide by singular integral equations," *Electron. Commun. Jpn. (Part I)*, Vol. 70, No. 6, 111–121, 1987.
20. Mittra, R., T. Itoh, and T. S. Li, "Analytical and numerical studies of the relative convergence phenomenon arising in the solution of an integral equation by the moment method," *IEEE Trans. Microwave Theory Tech.*, Vol. 20, No. 2, 96–104, 1972.
21. Geng, N. and L. Carin, "Wide-band electromagnetic scattering from a dielectric BOR buried in a layered lossy dispersive medium," *IEEE Trans. Antennas Propagat.*, Vol. 47, No. 4, 610–619, 1999.
22. Amitay, N. and V. Galindo, "On energy conservation and the method of moments in scattering problems," *IEEE Trans. Antennas Propagat.*, Vol. 17, No. 7, 747–751, 1969.
23. Hessel, A. and A. A. Oliner, "A new theory of Wood's anomalies on optical gratings," *Applied Optics*, Vol. 4, No. 10, 1275–1297, 1965.
24. Pozar, D. M., *Microwave Engineering*, 4th Edition, John Wiley & Sons, 2012.
25. Kundracik, F., M. Kocifaj, G. Videen, and J. Klačka, "Effect of charged-particle surface excitations on near-field optics," *Applied Optics*, Vol. 54, No. 22, 6674–6681, 2015.
26. Klačka, J., M. Kocifaj, F. Kundracik, G. Videen, and I. Kohut, "Generalization of electromagnetic scattering by charged grains through incorporation of interband and intraband effects," *Optics Letters*, Vol. 40, No. 21, 5070–5073, 2015.
27. Bleszynski, E., M. Bleszynski, and T. Jaroszewicz, "Surface-integral equations for electromagnetic scattering from impenetrable and penetrable sheets," *IEEE Antennas Propag. Mag.*, Vol. 35, No. 6, 14–25, 1993.
28. Ji, X., D. Sakomura, A. Matsushima, and T. Suyama, "Light scattering from two-dimensional periodic arrays of noble-metal disks and complementary circular apertures," *Progress In Electromagnetics Research M*, Vol. 43, 119–133, 2015.